The spectrum of antimony hydride: An ab initio configuration interaction study employing a relativistic effective core potential

Aleksey B. Alekseyev, Heinz-Peter Liebermann, Rainer M. Lingott, Ota Bludský, and Robert J. Buenker

Citation: The Journal of Chemical Physics **108**, 7695 (1998); doi: 10.1063/1.476205
View online: http://dx.doi.org/10.1063/1.476205
View Table of Contents: http://scitation.aip.org/content/aip/journal/jcp/108/18?ver=pdfcov
Published by the AIP Publishing

The spectrum of antimony hydride: An *ab initio* configuration interaction study employing a relativistic effective core potential

Aleksey B. Alekseyev, Heinz-Peter Liebermann, Rainer M. Lingott, Ota Bludský,[a] and Robert J. Buenker
Bergische Universität-Gesamthochschule Wuppertal, Fachbereich 9-Theoretische Chemie, Gaussstr. 20, D-42097 Wuppertal, Germany

(Received 7 January 1998; accepted 3 February 1998)

An *ab initio* configuration interaction (CI) study including the spin–orbit interaction is carried out for numerous valence and Rydberg states of the SbH radical by employing a relativistic effective core potential for the antimony atom. The computed spectroscopic constants are in good agreement with available experimental data, with a tendency toward a slight overestimation of bond lengths (by 0.01–0.03 Å) and T_e values (by 370–550 cm^{-1}) for the lowest singlet states. Measured excitation energies and spin–orbit splittings for the $A\ ^3\Pi$ multiplet are also accurately reproduced in the present calculations and the $\Omega=0^-$, 1, and 2 components of this state are shown to be strongly predissociated due to spin–orbit interaction with the corresponding components of the repulsive $^5\Sigma^-$ state. The most stable representative of the $A\ ^3\Pi$ multiplet, $A_4 0^+$, is found to possess a very unusual potential curve with a double minimum and a fairly low barrier to dissociation. Based on a vibrational analysis of this state it is concluded that the earlier observed $B0^+$ and $C0^+$ electronic states should be attributed to the $v=0$ and 2 vibrational levels of the $A_4 0^+$ state, while the state experimentally assigned as $A\ ^3\Pi_{0^+}$ corresponds to the $A_4 0^+$, $v=1$ level. Dipole moments $\mu(v=0)$ for the $\ldots\sigma^2\pi^2\ X^3\Sigma^-$, $a\ ^1\Delta$ and $b\ ^1\Sigma^+$ states are computed to have small (e.g., -0.238 D for $X_1\ ^3\Sigma^-_{0^+}$) and nearly equal negative values (Sb^+H^- polarity). The dipole transition moments and the corresponding radiative lifetimes for a number of low-energy electronic transitions have also been computed. Many other bound states and avoided crossings are indicated in the calculations which may be of relevance in future experimental studies of this system. © *1998 American Institute of Physics.* [S0021-9606(98)01218-5]

I. INTRODUCTION

While the two lightest representatives of the Group VA diatomic hydrides, NH and PH, have been a subject of numerous experimental and theoretical investigations (see reviews[1,2] and references therein), much less is known about the heavier isovalent systems AsH, SbH, and BiH, with the SbH radical probably being the least studied of them.

The first spectroscopic observations of SbH have been reported by Bollmark and Lindgren,[3] and Basco and Yee,[4] who attributed absorption spectra measured after flash photolysis of stibine and deuterostibine to the $A\ ^3\Pi \leftarrow X\ ^3\Sigma^-$ transitions in SbH and SbD. The $A\ ^3\Pi \leftarrow X\ ^3\Sigma^-$ rotational structure has later been analyzed in more detail[5] and it has been concluded on this basis that there is one more 0^+ state in SbH and two others in SbD which lie in the same energy range as the $A\ ^3\Pi$ multiplet. Bollmark *et al.*[6] have also employed the same experimental approach to study absorption spectra of SbH and SbD in the vacuum ultraviolet region and have found a number of higher-lying electronic states of these radicals. More recently, Stackmann *et al.*[7] and Urban *et al.*[8] have used laser spectroscopy methods to measure infrared spectra of the $X\ ^3\Sigma^-$ ground state of the four ^{121}SbH, ^{123}SbH, and ^{121}SbD, ^{123}SbD isotopomers and have determined accurate spectroscopic constants.

The scope of experimental information available for the low-lying states of the Group VA diatomic hydrides has been significantly increased by Fink and co-workers,[9–13] who systematically studied the $a\ ^1\Delta$, $b\ ^1\Sigma^+ \rightarrow X\ ^3\Sigma^-$ transitions in these systems and determined spectroscopic constants for the metastable singlet states involved. These data provide new opportunities for testing the precision of *ab initio* calculations for molecules with heavy atoms. This is especially interesting for the SbH radical, for which the $a\ ^1\Delta$ and $b\ ^1\Sigma^+$ states have been observed by this group for the first time.[12,13]

The only *ab initio* calculation of SbH available to date has been carried out by Balasubramanian *et al.*[14] A relativistic effective core potential (RECP) has been employed for the Sb atom in this study, and potential curves for the nine lowest Ω states have been computed at the configuration interaction (CI) level including the spin–orbit interaction. This paper provides a reasonably good theoretical description of the SbH low-energy electronic spectrum, though the use of a somewhat small basis set and a limited CI treatment made it difficult to obtain accurate equilibrium distances, vibrational frequences, and excitation energies.

The main goal of the present study is to carry out systematic calculations of potential energy curves, transition moments and radiative lifetimes for the valence and Rydberg

[a]Present address: J. Heyrovský Institute of Physical Chemistry, Academy of Sciences of Czech Republic, CZ-18223 Prague 8, Czech Republic.

TABLE I. Excitation energies and spin–orbit splittings ΔE (in cm^{-1}) of the lowest-lying states of the Sb atom obtained in the present study in comparison with experimental data.[a]

			Calc.		Expt.	
Config.	Design.	J	Energy	ΔE	Energy	ΔE
$5s^25p^3$	$^4S^o$	3/2	0			
$5s^25p^3$	$^2D^o$	3/2	9 254		8 512	
				1 214		1 342
		5/2	10 468		9 854	
$5s^25p^3$	$^2P^o$	1/2	17 100		16 396	
				1 720		2 069
		3/2	18 820		18 465	

[a]Reference 22.

states of SbH within a computational scheme which consistently involves spin–orbit coupling. For this purpose a relativistic CI approach is employed which has recently been developed in our laboratory and is based on RECPs. Similar calculations have recently been carried out for the isovalent BiH (Ref. 15) and AsH (Ref. 16) radicals as well as for Sb-containing diatomics such as SbF,[17] SbO,[18] and SbI (Ref. 19) and have provided a reliable description of the electronic structure of these systems. A special emphasis in the present work is made on the analysis of the $A\ ^3\Pi$ multiplet, in particular its 0^+ component, as well as other 0^+ states which can possibly lie in the same energy range. Close attention is also paid to the strengths of the various radiative transitions, with the hope that these data may be useful in future experimental studies of the SbH radical.

II. DETAILS OF THE THEORETICAL TREATMENT

In the present theoretical treatment the core electrons of the antimony atom are described by a RECP given by LaJohn *et al.*,[20] with only the $5s$ and $5p$ electrons treated explicitly via basis functions. This choice of the RECP is based on our previous experience with calculations for the other Sb-containing diatomics,[17–19] in which the same RECP has been employed.

The $3s3p$ Cartesian Gaussian basis set recommended for use with the Sb RECP on the basis of SCF optimization[20] has been taken as a starting point in the present study. It has been augmented by one $s(0.07\ a_0^{-2})$, one $p(0.03\ a_0^{-2})$, two d (0.18 and 0.04 a_0^{-2}), and two f (0.34 and 0.11 a_0^{-2}) functions optimized in the atomic CI calculations of the $5s^25p^3\ ^4S^o$, $^2D^o$, and $^2P^o$ states. It was also necessary to add diffuse $s(0.013\ a_0^{-2})$ and $p(0.010\ a_0^{-2})$ functions to describe low-lying Rydberg states in the SbH spectrum, so that the final basis set for the Sb atom consists of $5s5p2d2f$ functions employed in uncontracted form. The AO basis set for the hydrogen atom is the $(8s2p)/[5s2p]$ set of Lie and Clementi[21] augmented by diffuse $s(0.0195\ a_0^{-2})$ and $p(0.042\ a_0^{-2})$ functions.

Results of the atomic test calculations, performed primarily for the Sb AO basis set optimization, are presented in Table I for the lowest $^4S^o$, $^2D^o$, and $^2P^o$ states in comparison with the experimental data from Moore.[22] One can see that a fairly high level of correlation treatment is achieved in the present study, though the $^2D^o$ and $^2P^o$ states still lie about 700 cm^{-1} higher than found experimentally. A similar overestimation has been obtained in our recent AsH study[16] as well, and it can be explained by common difficulties in correlating states of low multiplicity with the same accuracy as those of higher spin. Table I also shows reasonably good agreement between the calculated and experimental spin–orbit splittings for the $^2D^o$ and $^2P^o$ states of Sb, with a slight tendency to underestimate them in the present study.

The first step in the theoretical treatment of the SbH radical is a SCF calculation of the $^3\Sigma^-(\ldots\sigma^2\pi^2)$ ground state. The resulting SCF-MOs are then used as orthonormal basis for the ensuing CI calculations. All computations are carried out in formal C_{2v} symmetry in order to take advantage of the simplicity of the Abelian group direct product relationships. The conventional multireference single- and double-excitation (MRD-CI) method[23] is employed to obtain eight roots for every singlet and triplet symmetry, as well as two roots for $^5A_2$ and one for each of the degenerate $^5B_1$ and $^5B_2$ symmetries. At this stage of the calculations the SO interaction is neglected, but other relativistic effects are included through the spin-independent part of the Sb RECP. Results are obtained at 80 internuclear distances in the interval from 2.3 to 10.0 a_0, with an increment of 0.03–0.05 a_0 in the Franck–Condon range (2.9–5.25 a_0) and at representative shorter and longer bond lengths. Calculations at such a large number of internuclear distances are needed to accurately describe numerous avoided crossings between electronic states characteristic for the SbH radical. A series of key reference configurations is chosen for each of the low-lying SbH roots at different distances, and these reference sets are used for each Λ–S symmetry for the whole range of internuclear separations considered in order to obtain smooth potential curves at approximately the same level of accuracy. A perturbative selection procedure is employed to reduce the sizes of the secular equations, with a selection threshold T of 2 μs for all symmetries and distances. Energy results at the unselected level of treatment ($T\rightarrow 0$) are then obtained by an extrapolation procedure,[23] while the effects of higher excitations are taken into account via a generalization of the Davidson correction.[24,25] Details concerning the sizes of secular equations treated may be found in Table II, as well as the numbers and symmetries of the roots obtained. The linear notation for the lowest two roots in each C_{2v} space is also given, along with the sums of squared coefficients of reference configurations Σc_p^2 in the corresponding final wave functions. The Table CI algorithm[26] is used in the computational scheme in order to deal efficiently with the complicated open-shell relationships which arise among the various pairs of selected configurations.

The next step in the present approach is to employ the Λ–S eigenfunctions as basis for the final spin–orbit calculations. For this purpose the spatial functions are multiplied with appropriate spin functions and the Wigner–Eckart theorem is employed to compute spin–orbit matrix elements between them based on results obtained for representative pairs of S^2 eigenfunctions. The estimated full CI energies are placed on the diagonal of the Hamiltonian matrices, whereas the variational Λ–S wave functions are employed to calcu-

TABLE II. Technical details of the MRD-CI calculations for the SbH molecule at $T=2\ \mu E_h$.[a]

C_{2v}	$N_{\rm ref}/N_{\rm root}$	SAFTOT/SAFSEL	$C_{\infty v}$	Σc_p^2
$^1A_1$	155/8	730512/18255	$^1\Delta$	0.9342
			$^1\Sigma^+$	0.9303
$^1A_2$	140/8	881678/22126	$^1\Delta$	0.9351
			$^1\Sigma^-$	0.9245
$^1B_{1,2}$	144/8	803178/18434	$1\ ^1\Pi_{x,y}$	0.9225
			$2\ ^1\Pi_{x,y}$	0.9198
$^3A_1$	174/8	1568172/22470	$^3\Delta$	0.9283
			$^3\Sigma^+$	0.9270
$^3A_2$	109/8	1217811/21932	$^3\Sigma^-$	0.9379
			$^3\Delta$	0.9233
$^3B_{1,2}$	140/8	1338704/25548	$1\ ^3\Pi_{x,y}$	0.9288
			$2\ ^3\Pi_{x,y}$	0.9252
$^5A_2$	69/2	480846/8633	$1\ ^5\Sigma^-$	0.9341
			$2\ ^5\Sigma^-$	0.9377
$^5B_{1,2}$	84/1	669618/3682	$1\ ^5\Pi_{x,y}$	0.9385

[a]The number of selected SAFs and Σc_p^2 values are given for $r=3.27a_0$. SAFTOT designates the total number of generated, SAFSEL the number of selected SAFs. $N_{\rm ref}$ and $N_{\rm root}$ refer to the number of reference configurations and roots treated, respectively.

late the off-diagonal spin–orbit matrix elements. The orders of the corresponding secular equations are 34 for A_1 and B_1, and 36 for A_2. Since each B_2 function has a degenerate partner in B_1, it is not necessary to solve both these secular equations explicitly. More details of the theoretical treatment may be found elsewhere.[27,28]

The final stage of the present computational scheme involves fitting the resulting potential energy curves to polynomials which serve as the potentials in one-dimensional nuclear motion Schrödinger equations to be solved numerically.[29,30] The vibrational wave functions obtained are combined with transition moments for the Ω electronic states to compute Einstein coefficients for various pairs of vibrational states, from which the radiative lifetimes of individual upper-state levels are determined by summing over the transition probabilities to all lower-lying states and inverting.

III. POTENTIAL ENERGY RESULTS

A. $\Lambda-S$ potential curves

Potential energy curves obtained from the spin-independent CI calculations are plotted in Fig. 1 for all valence states converging to the three lowest Sb atomic states, $^4S^o$, $^2D^o$, and $^2P^o$, in combination with H(^2S), as well as for the two lowest Rydberg states, $3^{3,1}\Pi$. In the Franck–Condon region the most stable electronic configuration is the $\sigma^2\pi^2$ species, which gives the well-known series of three multiplets, $X\ ^3\Sigma^- < a\ ^1\Delta < b\ ^1\Sigma^+$. The $X\ ^3\Sigma^-$ state correlates with the $^4S^o$ ground state of the antimony atom, while the $a\ ^1\Delta$ and $b\ ^1\Sigma^+$ converge to $^2D^o$ and $^2P^o$, respectively. The only other molecular state converging to the Sb($^4S^o$) + H(^2S) limit is the $^5\Sigma^-$ of $\sigma\pi^2\sigma^*$ electronic configuration. It has a repulsive potential curve due to electron excitation from the bonding σ to the antibonding σ^* MO, but nevertheless plays an important role in the low-energy SbH spectrum, causing predissociation of the $A\ ^3\Pi$ multiplet.

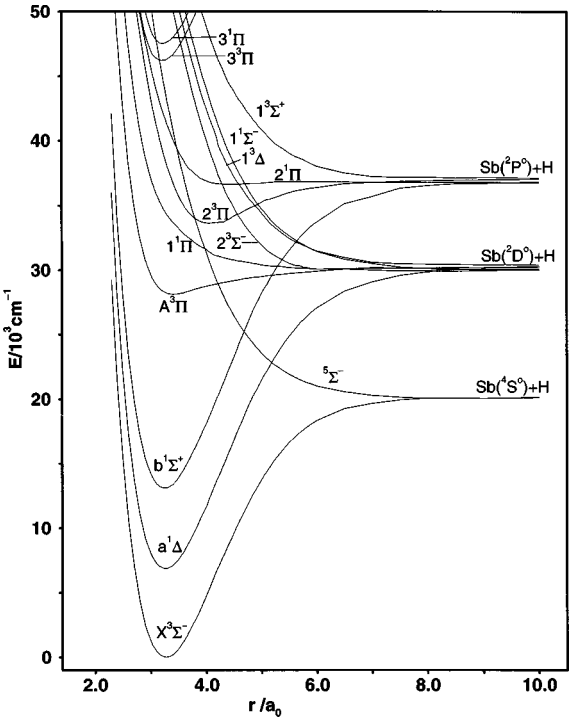

FIG. 1. Computed potential energy curves of the low-lying $\Lambda-S$ states of SbH obtained without inclusion of the spin–orbit interaction.

Similar to what was found earlier for BiH (Ref. 15) and AsH,[16] the next most stable states are two pairs of $^{3,1}\Pi$ species, originating from the $\sigma\pi^3$ and $\sigma^2\pi\sigma^*$ configurations. Both triplet states are bound, although quite weakly, by $\sim$2100 and $\sim$3400 cm^{-1}, respectively, while both singlets are repulsive. The second of them has a very flat potential curve at long distances, however, with a shallow minimum of about 200 cm^{-1} at $\simeq 4.45\,a_0$. As we have already mentioned in the AsH study,[16] such qualitative behavior of the low-lying $^{3,1}\Pi$ states is typical for the Group VA hydrides in general, but there exists an important quantitative difference in the strength of their bonding.

In the lightest of such systems, NH, both $\sigma\pi^3$ states, $A\ ^3\Pi$ and $c\ ^1\Pi$, are quite strongly bound, especially the $A\ ^3\Pi$ state, which has a binding energy of $\sim$2 eV and is only slightly shifted with respect to the ground state.[31,32] In the PH radical the $A\ ^3\Pi$ bonding energy is somewhat smaller, $\leqslant$1.5 eV,[33,34] and the $^1\Pi(\sigma\pi^3)$ state has never been observed, consistent with the rather flat potential curve obtained for it in the *ab initio* calculations.[33] From our recent AsH study[16] it follows that the $A\ ^3\Pi$ state is significantly less bound (by $\sim$3000 cm^{-1}) in AsH than in the two lighter homologues, while the $^1\Pi$ is repulsive. As one can see from Fig. 1, this trend also holds in SbH, for which the $A\ ^3\Pi$ binding energy is only $\sim$2100 cm^{-1} and the corresponding singlet state is repulsive. In the heaviest of the Group VA hydrides, BiH, neither of the $\sigma\pi^3\ ^{3,1}\Pi$ states has a minimum.[15] It should be noted that for the latter three systems we use our calculated data at the $\Lambda-S$ level of treatment in order to remove spin–orbit coupling effects and thus make comparison with the lighter radicals more straightforward.

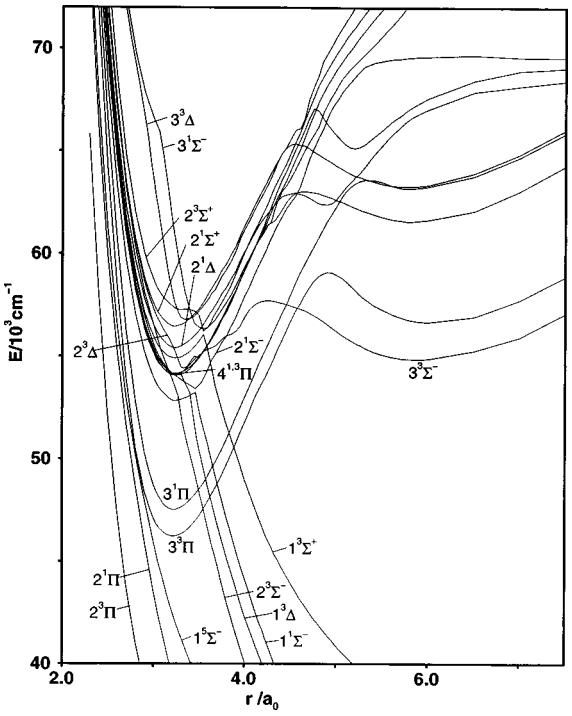

FIG. 2. Computed potential energy curves of the lowest Rydberg $\Lambda-S$ states of SbH obtained without inclusion of the spin–orbit interaction.

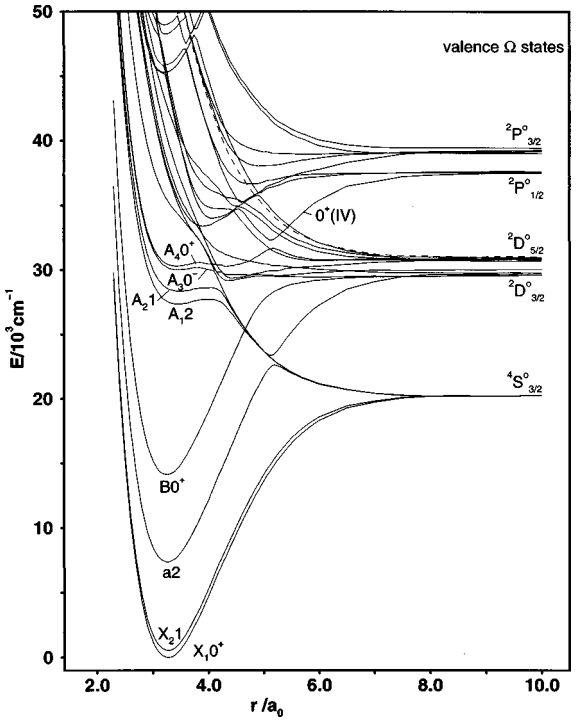

FIG. 3. Computed potential energy curves of the valence Ω states of SbH obtained after inclusion of the spin–orbit interaction.

The above trend can be explained in terms of the character of the σ and π MOs in this group of radicals. The σ orbital becomes less and less bonding toward the end of the row, while the π MO does not change much through this class of systems, being almost completely localized on the Group VA atom and therefore having nonbonding character. Thus the $\sigma\rightarrow\pi$ excitation causes less and less bonding in the $\sigma\pi^3$ $^{3,1}\Pi$ states of the heavier systems. These considerations lead to an immediate conclusion that an opposite trend must be observed for the $\sigma^2\pi\sigma^*$ $^3\Pi$ states, since the σ^* MO, which is the orthogonal complement to the σ, becomes less antibonding toward the end of the row. This assumption is supported by a comparison of our $\Lambda-S$ results for AsH and SbH. The binding energy of the $\sigma^2\pi\sigma^*$ $^3\Pi$ state in the former radical is calculated to be 2100 cm^{-1}, while in SbH it increases to 3400 cm^{-1}. One can note, however, that the situation with the 2 $^3\Pi$ state is actually more complicated, since contributions to this state from the $\sigma\pi^3$ and $\sigma^2\pi\sigma_R$ are also important, and thus a simple qualitative analysis based on a one-configuration approach is not quite adequate.

Potential energy curves for four more valence states, 2 $^3\Sigma^-$, 1 $^3\Delta$, 1 $^1\Sigma^-$, and 1 $^3\Sigma^+$, are presented in Fig. 1. The first three of them go to the Sb($^2D^o$)+H(^2S) atomic limit, while the 1 $^3\Sigma^+$ dissociates to Sb($^2P^o$)+H(^2S). All these states stem from the same $\sigma\pi^2\sigma^*$ configuration as the $^5\Sigma^-$ state discussed earlier and therefore are repulsive.

The range of excitation energies from 40 000 to 70 000 cm^{-1} is shown in Fig. 2 to focus on the low-lying Rydberg states of SbH. The lowest pair of them, $3^{3,1}\Pi$, arises from the $\sigma^2\pi\sigma_R$ configuration, but there are some other configurations such as $\sigma\pi^2\sigma_R$, $\sigma^2\pi\pi_R$ or $\sigma^2\pi\sigma_R^*$ which result in numerous Rydberg states of various symmetries in this energy range. As may be expected, all of them are characterized by deep minima and equilibrium distances which are approximately equal to that of the X $^3\Sigma^-$ ground state, but there are many avoided crossings with the repulsive valence states, producing a complicated appearance for the potential diagram in this range.

B. Potential energy results for Ω states

After adding spin–orbit coupling to the theoretical treatment the $\Lambda-S$ states discussed above split into various components characterized by the Ω quantum number. Potential energy curves for the valence Ω states are shown in Fig. 3, and separately for each of the Ω values from 0^+ to 2 in Figs. 4–7, in which the Rydberg states are also included. The present computed spectroscopic constants for the low-lying Ω states are given in Table III, together with available experimental and previous theoretical values for these quantities. Though the spin–orbit interaction is fairly strong in the SbH radical, most of the low-lying electronic states have a well-defined $\Lambda-S$ origin. Therefore, in the following narration we shall use both a rigorous Ω notation as well as a less accurate $\Lambda-S$ one to underline the origin of the states to be discussed.

1. The ...$\sigma^2\pi^2$ states

The X $^3\Sigma^-$ ground state is split into 0^+ and 1 components. This splitting is calculated to be 541 cm^{-1}, somewhat smaller than the experimental value of 666.8 cm^{-1}.[8] As in the lighter isovalent AsH radical, this splitting is mainly caused by the spin–orbit interaction with the b $^1\Sigma^+$ state, which lowers the energy of the 0^+ ground state component by $\sim$590 cm^{-1}, with two other important contributions coming from the 1 $^3\Pi$ and 2 $^3\Pi$ states (33 and 15 cm^{-1}, respec-

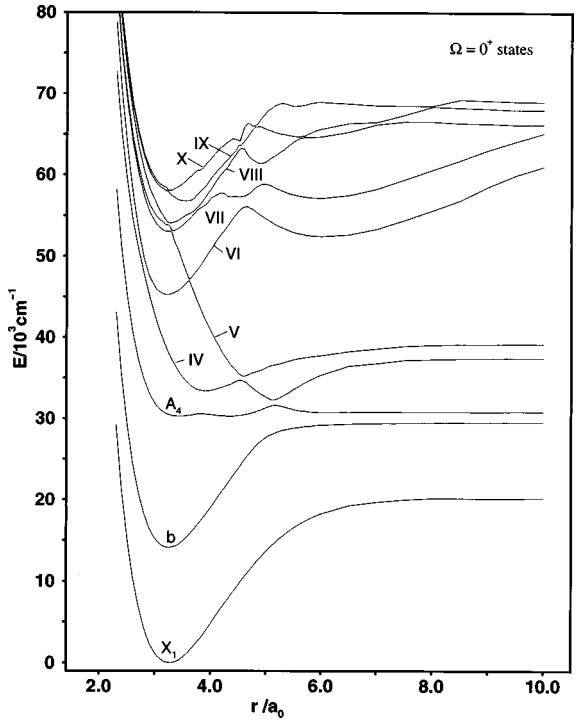

FIG. 4. Computed potential energy curves for the ten lowest $\Omega=0^+$ states of the SbH radical.

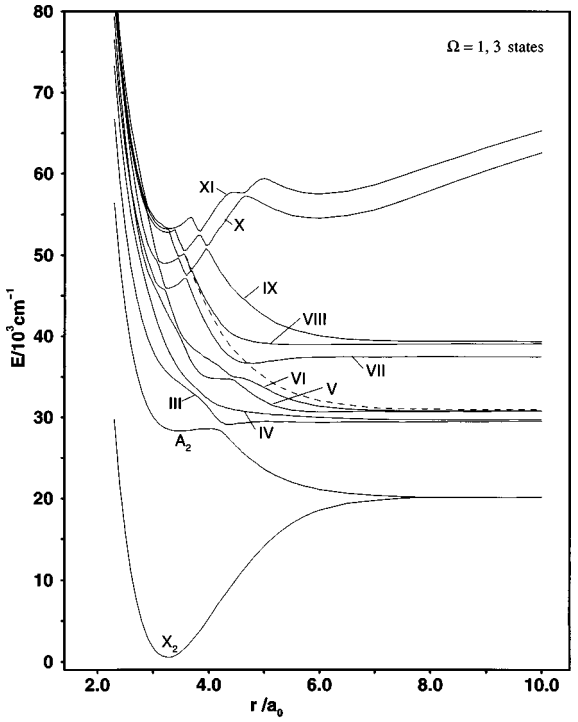

FIG. 6. Computed potential energy curves for the eleven lowest $\Omega=1$ states of the SbH radical. The dashed curve corresponds to the lowest $\Omega=3$ state of the system.

tively). All in all, the $^3\Sigma^-_{0^+}$ state energy is lowered by 662 cm^{-1} relative to the $\Lambda-S$ result, while the $^3\Sigma^-_1$ component goes down by 121 cm^{-1}, mainly due to the interaction with the lowest $^3\Pi$ and $^1\Pi$ states. As was pointed out earlier for the AsH radical,[16] there are two main reasons responsible for the underestimation of the ground state splitting. As one can see from the Sb atomic tests (Table I), there is a tendency to underestimate spin–orbit splittings of the Sb $^2D^o$ and $^2P^o$ states and this should lead to underestimation of the corresponding spin–orbit matrix elements in the SbH radical. The second reason is a slight overestimation of the $^1\Sigma^+$ energy, which also leads to a weaker coupling with the $X\ ^3\Sigma^-$ state. These two factors acting in concert produce the final

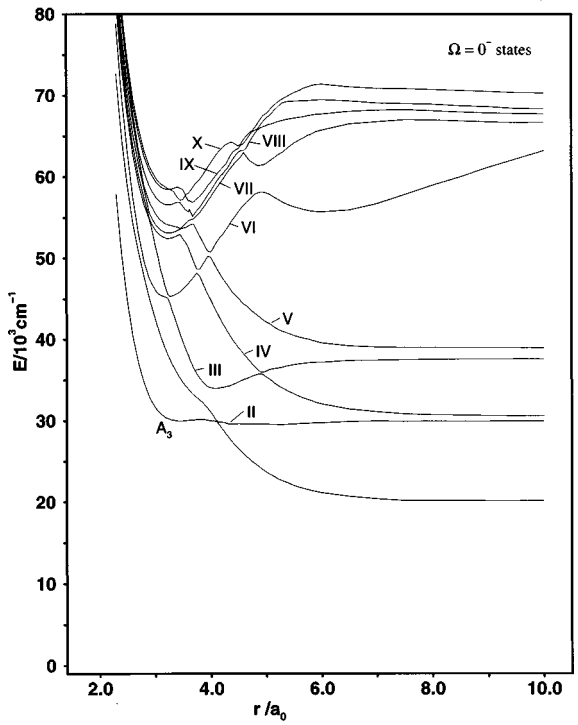

FIG. 5. Computed potential energy curves for the ten lowest $\Omega=0^-$ states of the SbH radical.

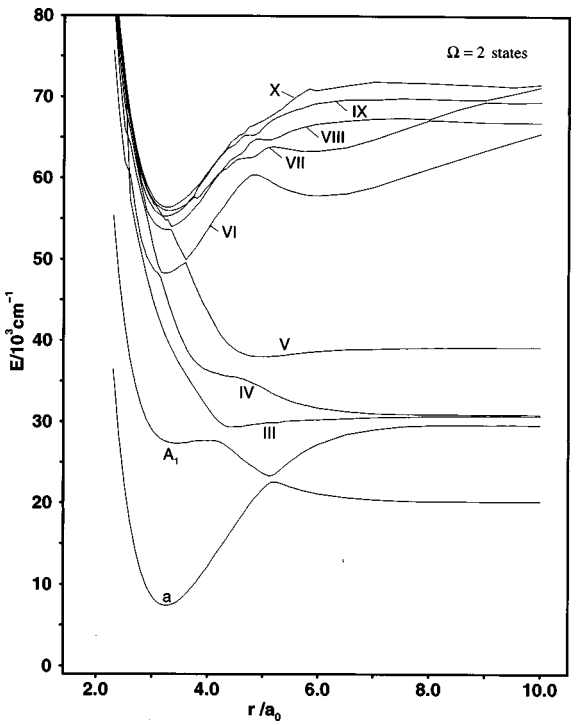

FIG. 7. Computed potential energy curves for the ten lowest $\Omega=2$ states of the SbH radical.

TABLE III. Calculated and experimental spectroscopic constants of SbH (transition energies T_e, bond lengths r_e, and vibrational frequencies ω_e).

	T_e/cm^{-1}		r_e/Å		ω_e/cm^{-1}	
State	Calc.	Expt.	Calc.	Expt.	Calc.	Expt.
$X_1\ ^3\Sigma^-_{0^+}$	0	0	1.731	1.717 3[a] [8]	1886	1923 [8]
			1.81 [14]		1763 [14]	
$X_2\ ^3\Sigma^-_1$	541	666.6 [8]	1.730	1.701 87 [12]	1892	
	696 [14]		1.81 [14]		1762 [14]	
$a\ ^1\Delta_2$	7 378	6 832 [12]	1.725	1.714 47 [12]	1904	1942 [13]
	9 362 [14]		1.81 [14]		1784 [14]	
$b\ ^1\Sigma^+$	14 129	13 752 [13]	1.721		1937	1950 [13]
	15 772 [14]		1.80 [14]		2061 [14]	
$A_1\ ^3\Pi_2$	27 307	27 301[b] [5]	1.820		1180	
$A_2\ ^3\Pi_1$	28 313		1.831		1121	
$A_3\ ^3\Pi_{0^-}$	30 007		1.826			
$A_4\ ^3\Pi_{0^+}$	30 255	30 449[c] [5]	1.820[d]			
	30 788 [14]		1.87 [14]		1085 [14]	
0^+ (IV)	33 402[e]		2.073		1308	
	32 324		2.719		1936	
	34 891 [14]					
0^+ (V)	45 257		1.704		2013	

[a]r_e value is calculated employing the B_e value from Ref. 8 and should be taken as an average value for the X_1 and X_2 ground state components (see text).
[b]T_e value estimated on the basis of the T_0 result from Ref. 5 (see text).
[c]T_e value estimated on the basis of the T_0 result for $B0^+$ from Ref. 5 (see text).
[d]r_e value for the left minimum of the $A_4 0^+$ potential curve.
[e]Entries in this line correspond to the left minimum of the 0^+ (IV) potential curve, in the line below, to the right minimum of this curve.

discrepancy of $\sim 126\ \text{cm}^{-1}$ with the experimental result.

The r_e values computed for the X_1 and X_2 ground state components are 1.731 and 1.730 a_0, respectively, and they agree well with the experimental value of 1.7173 a_0 estimated in the present work employing the B_e value from Ref. 8. The experimental r_e value should be considered as an average for the X_1 and X_2 states, since it was obtained from the infrared spectrum fitting in which $X\ ^3\Sigma^-$ was treated as a single state split by the spin–orbit interaction. The r_e value for the X_2 state determined in the recent study[12] of the $a\ ^1\Delta \rightarrow X_2\ ^3\Sigma^-_1$ emission is 1.701 87 a_0, which somewhat surprisingly is noticeably smaller than both the present calculated and previous experimental results.[8] An important difference between Refs. 8 and 12 is that in the rotational analysis of the $a \rightarrow X_2$ spectrum carried out in Ref. 12, the $X_2 1$ component has been treated as a separate state. If we assume that both experimental r_e values are reliable, the only possible explanation is that some nonadiabatic effects, presumably spin-rotation coupling, are important for accurate determination of the $X_{1,2}$ equilibrium distances. Such effects have been averaged in the fitting procedure of Ref. 8 and simply have not been considered in the present theoretical analysis performed at the adiabatic level. The computed vibrational frequency ω_e of the X_1 state is $37\ \text{cm}^{-1}$ smaller than the experimental result,[8] with a slight underestimation of the ω_e values being typical for the present study. It still means a noticeable improvement in comparison with the only other theoretical result available,[14] which is $160\ \text{cm}^{-1}$ lower than the experimental value. The ground $X_1\ ^3\Sigma^-_{0^+}$ state dissociation energy D_e has been estimated in the present study as the average of all five Ω roots (two for $X\ ^3\Sigma^-$ and three for $^5\Sigma^-$) going to the lowest $\text{Sb}(^4S^o)+\text{H}(^2S)$ dissociation limit. The D_e value obtained in this way is 2.52 eV, but no experimental result is available for comparison.

The lowest singlet state of SbH, $a\ ^1\Delta$, is calculated to lie $7378\ \text{cm}^{-1}$ above the ground state, $546\ \text{cm}^{-1}$ higher than found experimentally.[12] Such an overestimation may be anticipated on the basis of the Sb atomic tests (Sec. II) as well as our earlier AsH calculations,[16] in which a similar effect has been observed. The computed r_e value for the $a\ ^1\Delta$ state is 0.006 Å smaller than that for the X_1 state, and such a shortening of the $a\ ^1\Delta$ state equilibrium distance with respect to the ground state has also been found experimentally[12] (Table III). It can be qualitatively explained by the fact that the $a\ ^1\Delta$ state converges diabatically to the $\text{Sb}(^2D^o)$ limit, which lies $8512\ \text{cm}^{-1}$ higher than $^4S^o$ and thus should have a steeper attractive limb for its potential curve than X_1. This also explains the somewhat higher vibrational frequency determined for this state, both theoretically (by $18\ \text{cm}^{-1}$) and experimentally (by $19\ \text{cm}^{-1}$), as compared to the X_1 ω_e value. On its way to the dissociation limit the $a\ ^1\Delta$ state undergoes an avoided crossing with the repulsive $^5\Sigma^-$ state, which leads to a barrier for its potential curve at $r \simeq 5.2\ a_0$ and, as a result, to convergence of the lowest $\Omega=2$ state to the $\text{Sb}(^4S^o)+\text{H}(^2S)$ dissociation limit.

The excitation energy for the highest of the $\ldots\sigma^2\pi^2$ states, $b\ ^1\Sigma^+$, is calculated to be $14\,129\ \text{cm}^{-1}$, in good agreement with the measured value of $13\,752\ \text{cm}^{-1}$.[13] The computed r_e value for this state is 0.01 Å shorter than that of the $X_1 0^+$ ground state due to the same reasons discussed

above for the $a\ ^1\Delta$ state. Moreover, the direct spin–orbit interaction between $b\ ^1\Sigma^+$ and $X_1\ ^3\Sigma^-_{0+}$, which increases with distance, may only lead to a further shortening of the upper state r_e value, which effect, however, is very small. The calculated ω_e value is 1937 cm^{-1} and agrees well with the observed result of 1942 cm^{-1}.[13]

2. The $A\ ^3\Pi$ multiplet

The $A\ ^3\Pi$ multiplet is without doubt the most interesting state in the low-energy SbH spectrum and the spin–orbit interaction plays a crucial role in its spectroscopic properties. As discussed in Sec. III A, it predominantly arises from the $\ldots\sigma\pi^3$ electronic configuration and thus has the inverse ordering of Ω components. Three of them are strongly predissociated due to spin–orbit coupling with the corresponding $^5\Sigma^-$ components and therefore have very shallow minima. This leads to significant difficulties in their experimental observation and especially in obtaining accurate spectroscopic constants for these states. According to our calculations, the T_e value for the lowest $A_1\ ^3\Pi_2$ state (the A_i states have their indices $i=1,...,4$ according to increasing energy) is 27 307 cm^{-1}, and its potential well is only $\sim$400 cm^{-1} deep. This is enough to support one vibrational level in the SbD isotopomer, but none is predicted for the SbH system. This theoretical finding is in good qualitative agreement with the results of the experimental study,[5] in which sharp rotational lines have been observed in the $A_1\ ^3\Pi_2,\ v'=0\leftarrow X_2\ ^3\Sigma^-_1$ absorption spectrum of SbD, and the corresponding transition in SbH has been found to be strongly predissociated. For this reason it was not possible to determine the T_e value for the A_1 state but rather only the T_0 quantity for the SbD radical.[5] Employing this T_0 value together with the experimental energy of the $X_2\ ^3\Sigma^-_1,\ v''=0$ level from Ref. 8 and the calculated energy of the $A_1\ ^3\Pi_2,\ v'=0$ level from the present study, we can estimate an experimental T_e value for the $A_1\ ^3\Pi_2$ state to be 27 301 cm^{-1}, in very good agreement with the present calculated result. Unfortunately, no comparison with experimental data is possible for the r_e and ω_e quantities since no reliable values can be estimated for them, with only the one vibrational level having been observed for SbD.

It was not possible in Ref. 5 to determine the T_0 value for the $A_2\ ^3\Pi_1$ state due to its strong predissociation and not a single band could be interpreted as an excitation to the $A_3\ ^3\Pi_{0^-}$ state. The corresponding T_e values calculated in the present study are 28 313 and 30 007 cm^{-1} for A_2 and A_3, respectively. The computed bond lengths for A_i $(i=1,2,3)$ differ very little and lie in the 1.82–1.83 Å interval. This is 0.09–0.10 Å longer than for the ground state, which is consistent with the fact that the $A\ ^3\Pi$ multiplet arises from a $\sigma\rightarrow\pi$ excitation relative to the $\sigma^2\pi^2$ ground state configuration. The ω_e values for all A_i states (Table III) are noticeably smaller than that of the ground state, also consistent with the quite weak bonding characteristic of the $A\ ^3\Pi$ multiplet.

The highest $A\ ^3\Pi$ component, $A_4 0^+$, possesses a very unusual potential curve (see Figs. 3 and 4) and requires some special analysis together with the other 0^+ states, as will be done in the next section.

TABLE IV. Composition of the five lowest 0^+ states of SbH (c^2, %) at various bond distances r (in a_0).

State	r	$1\ ^3\Sigma^-$	$2\ ^3\Sigma^-$	$1\ ^1\Sigma^+$	$1\ ^3\Pi$	$2\ ^3\Pi$	$3\ ^3\Pi$
$X_1 0^+$	2.8	95.9		3.9			
	3.27	95.8		3.9			
	4.0	95.5		4.0			
	6.0	95.7		2.8		1.1	
	10.0	96.8		2.0			
$b 0^+$	2.8	3.7		95.3	1.0		
	3.27	3.8		95.1	1.0		
	4.0	4.0		93.3	2.5		
	5.0	3.2	1.4	54.1	40.2		
	6.0	1.8	19.2	11.7	64.5	2.8	
	10.0	1.2	29.4	7.6	57.3	3.5	
$A_4 0^+$	2.8				98.8		
	3.45			1.0	98.7		
	3.9			2.1	92.3	5.4	
	4.4			6.8	84.1	9.0	
	5.0		2.3	38.5	53.2	5.4	
	5.2		61.4	14.8	22.9		
	10.0		63.0		36.5		
0^+ (IV)	3.27					99.7	
	3.9				5.6	93.8	
	4.5		9.5		8.1	81.7	
	4.7		94.0			5.1	
	5.15		57.7	29.2	7.7	5.0	
	6.0		2.3	77.3	5.3	14.2	
	10.0			42.1		57.7	
0^+ (V)	2.8						99.7
	3.27						99.7
	3.7		99.9				
	4.4		98.4			1.4	
	4.7		5.7		7.1	86.1	
	6.0	1.6	2.2	8.0	6.1	81.9	
	10.0	1.7	4.7	42.5	6.5	43.6	

3. The $A_4 0^+$ state and higher-lying 0^+ states

The $A_4 0^+$ potential curve has two minima which are separated by a small barrier, $\sim$290 cm^{-1} high with respect to the left minimum, which occurs at $r_e=3.44\ a_0$. The right minimum at $r=4.32\ a_0$ has even a bit lower (by $\sim$35 cm^{-1}) energy and this gives a T_e value for the $A_4 0^+$ state of 30 255 cm^{-1}. Once again, as has been done earlier for the $A_1\ ^3\Pi_2$ component, we can estimate the corresponding experimental T_e value employing spectroscopic data from Ref. 5. For reasons which are given below, we use the T_0 value for the $B 0^+$ state for this purpose. This gives $T_e=30\ 449\ cm^{-1}$, in good agreement with the theoretical finding for the $A_4 0^+$ state. The $A_4 0^+ - A_1 2$ spin–orbit splitting is calculated in the present study to be 2948 cm^{-1} which also agrees quite well with the experimental value of 3148 cm^{-1}. At larger internuclear distances, the $A_4 0^+$ potential curve possesses a barrier to dissociation with a maximum of 31 660 cm^{-1} lying at 5.15 a_0. A better understanding of the reasons for such a complicated shape of the $A_4 0^+$ potential curve can be obtained from Table IV, in which the $\Lambda-S$ composition of the five lowest 0^+ roots is given. At short internuclear distances up to a small hump in the middle of its potential well at approximately 3.9 a_0, the $A_4 0^+$ state is dominated by the $1\ ^3\Pi(\ldots\sigma\pi^3)$ state. At this point the influence of the $2\ ^3\Pi$ and $b\ ^1\Sigma^+$ states becomes noticeable, with the former state at first making a somewhat stronger contri-

TABLE V. Excitation energies (in cm^{-1}) for vibrational levels of the $A_4 0^+$ state calculated with respect to the $X_1\,{}^3\Sigma_{0^+}^-$, $v''=0$ state. Comparison is made with the experimental T_0 values for the A, B, and $C0^+$ states of SbH and SbD.[a]

SbH							SbD						
	Calc.			Expt.				Calc.			Expt.		
	v'	$E_{v'}$	ΔE	State	T_0	ΔE		v'	$E_{v'}$	ΔE	State	T_0	ΔE
$A_4 0^+$	0	29 605		$B0^+$	29 761		$A_4 0^+$	0	29 818		$B0^+$	29 960	
			368			355				192			200
	1	29 973		$A\,{}^3\Pi_{0^+}$	30 116			1	30 010		$A\,{}^3\Pi_{0^+}$	30 160	
			689							421			406
	2	30 662						2	30 431		$C0^+$	30 566	
										460			
								3	30 891				

[a]Reference 5.

bution which causes a decrease of the $A_4 0^+$ potential energy. At longer distances, however, the $b\,{}^1\Sigma^+$ contribution becomes increasingly important until an avoided crossing with the repulsive $2\,{}^3\Sigma^-$ state occurs at $\sim 5.15\ a_0$, after which the $A_4 0^+$ state dissociates to the $\mathrm{Sb}(^2D^o_{5/2}) + \mathrm{H}(^2S_{1/2})$ atomic limit.

Experimentally[5] two more absorption bands for SbD and one for SbH have been observed in the same spectral range and attributed to additional 0^+ electronic states, $B0^+$ and $C0^+$. The $B0^+$ state has been found to lie lower than $A_4 0^+$ in both systems at $T_0 = 29\,761\ cm^{-1}$ (SbH) and $29\,960\ cm^{-1}$ (SbD), while the $C0^+$ state (SbD) lies higher, at $T_0 = 30\,566\ cm^{-1}$ (Table V). The present calculations show that there are indeed two more 0^+ states (Fig. 4) lying not far in energy from the $A_4 0^+$, both of them, however, having higher excitation energy than A_4. The lower state, designated in this work as $0^+(IV)$, has a potential curve with two minima at 3.92 and at 5.14 a_0, 33 402 and 32 324 cm^{-1}, respectively. The higher one, $0^+(\mathrm{V})$, has a minimal potential energy of 35 328 cm^{-1} at 4.65 a_0. The calculated excitation energies for the $0^+(\mathrm{IV})$ and $0^+(\mathrm{V})$ states are too high, however, to be identified with $B0^+$ and $C0^+$ from Ref. 5. Since the energy intervals between two successive 0^+ states found experimentally are no greater than 400 cm^{-1} in any case, it is natural to suppose that these states correspond in fact to different vibrational levels in the very flat and complicated $A_4 0^+$ potential which could produce an irregular vibrational ladder. In order to check this hypothesis we have calculated vibrational levels in the $A_4 0^+$ potential well and their energies are given in Table V together with the experimental data from Ref. 5.

One can see from these results that although the calculated vibrational levels lie $\sim 140-160\ cm^{-1}$ lower than the corresponding T_0 values (it is difficult to expect better accuracy from the *ab initio* calculation in this case), the measured energy intervals between them are reproduced rather well, within 15 cm^{-1} for both radicals. We have found three stable vibrational levels in the $A_4 0^+$ potential well of SbH and four such levels for SbD, though only two and three levels, respectively, have been observed in Ref. 5. The highest vibrational levels, $v'=2$ (SbH) and 3 (SbD), lie just under the top of the barrier, by 45 cm^{-1} (SbH) and 90 cm^{-1} (SbD), however (these energies have been calculated for technical reasons with the use of a vertical potential wall at $r = 5.25\ a_0$, which forces stabilization). Even if these levels exist in reality, they should be strongly predissociated and hence, be difficult to observe experimentally. From the above analysis one may safely conclude that the $B0^+$ and $C0^+$ states found in Ref. 5 are in fact the $v'=0$ and 2 vibrational levels of the $A_4 0^+$ electronic state, while the $A\,{}^3\Pi_{0^+}$ T_0 value reported therein actually corresponds to the $v'=1$ level. If this conclusion is correct, then the $B0^+$ T_0 experimental value rather than that of the $A\,{}^3\Pi_{0^+}$ state should be identified with the $A_4 0^+$ calculated T_0 result, and this has been done in Table III.

4. Higher-lying Ω states

The energy range from 29 000 to 39 000 cm^{-1} is characterized by a high density of states of various Ω symmetries, a number of which, e.g., 0^-(III, IV), 1(III, VII), 2(III, V) (Figs. 5–7), have potential minima. It should be difficult to observe these states spectroscopically, however, due to the occurrence of numerous avoided and allowed crossings in this region which cause predissociation of the above states. The first and second $^1\Pi$ states are of special interest, since they are the only low-lying states of SbH connected with the metastable $a\,{}^1\Delta$ state by dipole-allowed transitions, which otherwise has only one weak transition down to the $X_2\,{}^3\Sigma^-$ state. The present calculations show, similarly as to what has been found earlier for AsH,[16] that both $^1\Pi$ states are repulsive and therefore it is highly unlikely that $1,2\,{}^1\Pi \rightarrow a\,{}^1\Delta$ luminescence can be observed.

There is a gap in the SbH electronic spectrum from 39 000 to 45 000 cm^{-1}, at which energy the first Rydberg state appears, $3\,{}^3\Pi(\sigma^2\pi\sigma_R)$. As one can see from Figs. 3–7, this state is strongly bound and split by the SO interaction into Ω components with regular ordering. The splitting between the $\Omega=2$ and 0^+ substates is calculated to be $\sim 3000\ cm^{-1}$, approximately the same as for the $A\,{}^3\Pi$ multiplet. This is not surprising since it arises in both cases from spin–orbit matrix elements involving basically the same π MOs. The computed spectroscopic constants for the lowest 0^+ component of $3\,{}^3\Pi$ [the $0^+(\mathrm{V})$ state], which is almost

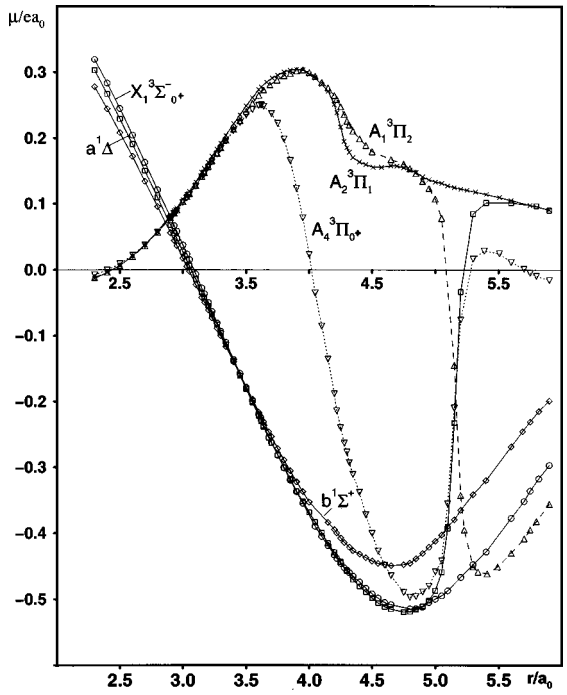

FIG. 8. Computed electric dipole moments for a number of low-lying states of the SbH radical. A positive value indicates a positive charge on the hydrogen atom.

almost degenerate with 0^-, are given in Table III. The 0^-, 1 and 2 substates are strongly predissociated near their minima (see Figs. 5–7) due to spin–orbit coupling with the corresponding $^5\Sigma^-$ components. The 0^+ substate seems to be the most stable multiplet, though it is also predissociated due to a potential crossing with the $2\,^3\Sigma^-$ state at $r=3.6\ a_0$.

The higher-lying Rydberg states, which have been observed[6] in the energy range of 56 450–62 800 cm^{-1}, lie too high to be reliably assigned in the present study, though there are a number of suitable candidates found in the calculations. For example, an electronic state with $T_0=58\,804\ cm^{-1}$ assigned as $F\ ^3\Pi_{0^+}$ in Ref. 6 may correspond to the $5\,^3\Pi_{0^+}(\sigma^2\pi\delta)$ state with a vertical excitation energy calculated to be 59 144 cm^{-1}. The experimentally observed $e\ ^1\Pi$ state ($T_0=56\,453\ cm^{-1}$) may be identified with the calculated $\Omega=1$ state (56 315 cm^{-1}), which is a mixture of $4\,^1\Pi$ and $4\,^3\Pi$, both arising from the same $\sigma^2\pi\sigma_R^{**}$ electronic configuration. There are six more $\Omega=1$ states in the 56 880–60 560 cm^{-1} energy interval, however, and the density of states for other symmetries is also quite high. For this reason and also because the accuracy of the present calculations decreases somewhat for such relatively high excitation energies, we will not comment further on this spectral range.

IV. DIPOLE MOMENTS AND RADIATIVE LIFETIMES

A. Electric dipole moments

Electric dipole moments μ computed for a number of low-lying electronic states are presented as a function of internuclear distance in Fig. 8. This figure is a nice illustration of the influence of spin–orbit coupling and CI on the electron density distribution and therefore merits a more detailed discussion.

As one can see from the figure, in the Franck–Condon region ($r\approx 2.7$–$4.0\ a_0$) the dipole moments of the $X_1\ ^3\Sigma^-_{0^+}$, $a\ ^1\Delta$, and $b\ ^1\Sigma^+$ states differ very little and have almost a linear dependence on the internuclear distance. This shows that the distribution of electronic density in all these states is mainly determined by their common $\sigma^2\pi^2$ electronic configuration, which is also confirmed by the structure of the CI wave functions and by comparison of the μ values calculated with and without including spin–orbit coupling. The dipole moments of all above states have small negative values at $r_e(X_1)=3.27\ a_0$: -0.0807, -0.0831, and $-0.0890\ ea_0$ for X_1, a, and b, respectively. This corresponds to Sb^+H^- polarity and shows that the electronic density in the bonding σ MO is slightly shifted towards the hydrogen atom at this distance. The situation is opposite to that in AsH,[16] for which small positive μ values for the X_1, a, and b states have been calculated at r_e, indicating a higher electronegativity of the As atom as compared to Sb. At smaller bond lengths ($r\leqslant 3.1\ a_0$), however, the dipole moments for all three states become positive due to a stronger localization of the σ MO on the antimony atom. At larger nuclear separations, dipole moment curves for all the above states reach their minima at $r\approx 4.7\ a_0$, after which the μ values naturally decrease as the SbH radical dissociates to neutral products, with somewhat larger differences in the μ values characteristic for the intermediate distances by virtue of the fact that the states discussed converge to three different atomic limits. The $a\ ^1\Delta$ state exhibits a sharply avoided crossing on its way to dissociation with the $^5\Sigma^-(\sigma\pi^2\sigma^*)$ state, which causes an abrupt change in its dipole moment in the $r=5.0$–$5.2\ a_0$ range of distances. Dipole moment values calculated for the lowest ($v=0$) vibrational levels of the $X_1\ ^3\Sigma^-_{0^+}$ and $X_2\ ^3\Sigma^-_1$ states are -0.0936 and $-0.0924\ ea_0$, respectively, which shows that the influence of the SO interaction on this property of the $X\ ^3\Sigma^-$ multiplet is very small in the Franck–Condon region. For this reason only the X_1 dipole moment curve is given in Fig. 8.

Unlike the $\sigma^2\pi^2$ states, all Ω components of the $A\ ^3\Pi$ multiplet (three of them are shown in Fig. 8) have positive dipole moment values in the Franck–Condon region, and they are considerably larger than for the states discussed first. This can be easily explained by the fact that the $A\ ^3\Pi$ state is predominantly characterized by the $\sigma\pi^3$ configuration at these distances, with the π MO being localized on the Sb atom. At short bond lengths the influence of the SO interaction on the dipole moment curves of the A_i substates is so small that they almost coincide up to $r=3.5\ a_0$. At larger distances the strong spin–orbit interaction of the $A_4 0^+$ substate with $2\,^3\Pi$ and $b\ ^1\Sigma^+$, both having negative μ values, leads to a fast decrease of the $A_4 0^+$ dipole moment and a change in its sign. At $r\approx 5.15\ a_0$ there is an avoided crossing between A_4 and $2\,^3\Sigma^-(\sigma\pi^2\sigma^*)$ which causes an abrupt change in the A_4 dipole moment, making it positive again. The $A_1\ ^3\Pi_2$ and $A_2\ ^3\Pi_1$ states do not interact with $b^1\Sigma^+$ because of symmetry and are much less influenced by the $2\,^3\Pi$ state than A_4 due to much larger differences in energies for the $\Omega=2$ and 1 components. A decrease in the dipole moments of these states in the range of 4.0–4.5 a_0 is caused by avoided crossings with the $^5\Sigma^-_{1,2}$ states. As a direct con-

TABLE VI. Computed transition dipole moments μ (in ea_0) between $X_1\ ^3\Sigma^-_{0^+}$, $X_2\ ^3\Sigma^-_1$, $a\ ^1\Delta$, $b\ ^1\Sigma^+$, and $A_i\ ^3\Pi_\Omega$ states of the SbH radical at various bond lengths r (in a_0).

r	$a-X_2$	$b-X_1$	$b-X_2$	A_1-X_2	A_1-a	A_4-X_1	A_4-X_2
2.70	0.010 77	0.002 47	−0.044 59	0.242 12	−0.013 37	−0.008 00	0.235 84
2.80	0.010 17	⋯	−0.042 03	0.232 11	−0.008 68	−0.004 77	0.226 61
2.90	0.009 73	⋯	−0.039 22	0.221 65	−0.003 91	−0.001 74	0.216 78
2.95	0.009 57	0.002 16	−0.038 09	0.216 60	−0.001 66	−0.000 09	0.212 25
3.00	0.009 30	0.002 49	−0.036 93	0.211 62	0.000 69	0.001 59	0.207 34
3.05	0.009 09	⋯	−0.035 81	0.206 41	0.002 92	0.003 11	0.202 43
3.10	0.008 86	0.001 70	−0.034 69	0.201 16	⋯	0.005 07	0.197 15
3.15	0.008 71	0.001 94	−0.033 50	0.195 54	0.012 40	0.006 74	0.191 76
3.20	0.008 51	0.002 00	−0.032 53	0.190 11	0.015 23	0.008 55	0.186 10
3.27	0.008 29	0.002 56	−0.030 84	0.181 68	0.019 27	0.011 47	0.177 66
3.34	0.008 05	0.002 76	−0.029 27	0.173 35	0.023 85	0.014 61	0.168 15
3.40	0.007 72	0.003 40	−0.027 91	0.166 24	0.027 41	0.017 96	0.159 98
3.45	0.007 51	0.004 09	−0.026 82	0.159 99	0.030 88	0.021 00	0.152 61
3.50	0.007 40	0.004 64	−0.025 83	0.154 13	0.034 16	0.024 36	0.144 12
3.55	0.007 20	0.005 28	−0.024 91	0.147 64	0.037 78	0.027 90	0.135 50
3.60	0.007 00	0.006 35	−0.024 01	0.141 26	0.041 39	0.032 31	0.126 60
3.64	0.006 75	0.007 22	−0.023 14	0.135 33	0.044 35	0.036 13	0.119 04
3.70	0.006 65	0.008 64	−0.022 01	0.128 72	0.048 58	0.043 82	0.107 18
3.75	0.006 58	0.009 70	−0.021 17	0.123 08	0.052 56	0.048 35	0.097 47
3.80	0.006 47	0.011 20	−0.020 18	0.115 99	0.057 36	0.054 18	0.085 13
3.85	0.006 31	0.012 42	−0.019 33	0.110 00	0.061 34	0.059 67	0.074 65
3.90	⋯	0.014 07	−0.018 66	0.103 36	0.065 69	0.110 51	0.063 27
4.00	0.006 05	0.018 57	−0.016 08	0.089 15	0.073 43	0.073 54	0.042 98
4.10	⋯	⋯	⋯	0.075 09	0.028 96	0.084 59	0.026 02
4.20	0.006 00	⋯	−0.015 74	0.055 96	0.074 28	0.096 38	0.013 46
4.25	0.005 60	0.032 69	−0.014 20	0.046 79	0.071 41	0.091 29	0.007 49

sequence of the Wigner–Eckart theorem the $A_2 1-{}^5\Sigma^-_1$ avoided crossing is the sharper of the two and this leads to a faster change of the $A_2 1$ dipole moment to the ${}^5\Sigma^-$ μ value as compared to the $A_1 2$ state. Unfortunately, no other experimental or theoretical data are available for the dipole moments of the SbH radical.

B. Transition moments and radiative lifetimes

Electric dipole transition moments for a series of low-energy radiative processes are given as a function of internuclear distance in Table VI. These dipole moment functions have been integrated over vibrational functions of the corresponding electronic states to obtain Einstein coefficients and radiative lifetimes, which are presented for the $v'=0$ levels of these states in Table VII.

As we have already seen in the previous sections, the $X\ ^3\Sigma^-$ ground state is relatively weakly influenced by the spin-orbit interaction, and as a consequence the calculated dipole moment values for the X_2-X_1 transition are very small, lying between 0.003 25 and 0.008 12 ea_0 in the Franck–Condon region. They are almost an order of magnitude larger than for the corresponding transition in the lighter AsH system, however, and the computed radiative lifetime for the X_2, $v'=0$ state is 105 s, much shorter than the extremely large value of 6×10^5 s estimated previously for the analogous state of AsH.[16] It is also possible that other effects not considered in the present study such as magnetic dipole transitions and nonadiabatic interactions may be important for obtaining the final radiative lifetime value for the X_2 state.

The $a\ ^1\Delta-X_2\ ^3\Sigma^-_1$ transition is both spin- and symmetry-forbidden at the $\Lambda-S$ level of treatment and therefore is also expected to be quite weak, as confirmed in the present calculations. As in the case of the AsH radical,[16] this transition mainly borrows its intensity from the $A\ ^3\Pi-X\ ^3\Sigma^-$ and $a\ ^1\Delta-1\ ^1\Pi$ transitions, but contributions from the higher-lying states are also not negligible. The computed radiative lifetime of the $a\ ^1\Delta(v=0)$ state is 23 ms, approximately four times shorter than calculated for AsH, which is again an indication of the noticeably stronger spin–orbit effects in the SbH radical. The $a-X_2$ transition has already been observed in emission,[12] but no experimental τ value is available for comparison with the calculated result.

The $b\ ^1\Sigma^+$ state has two dipole-allowed transitions to

TABLE VII. Calculated radiative lifetimes (in s) of excited states ($v'=0$) of SbH. Partial lifetimes τ_p for transitions to $X_1\ ^3\Sigma^-_{0^+}$, $X_2\ ^3\Sigma^-_1$, $a\ ^1\Delta$, and $b\ ^1\Sigma^+$, respectively, and total lifetime τ.[a]

State	$\tau_p(X_1)$	$\tau_p(X_2)$	$\tau_p(a)$	$\tau_p(b)$	τ
$X_2\ ^3\Sigma^-_1$	105	⋯	⋯	⋯	105
$a\ ^1\Delta$	⋯	23(−3)	⋯	⋯	23(−3)
$b\ ^1\Sigma^+$	16(−3)	105(−6)	⋯	⋯	104(−6)
$A_1\ ^3\Pi_2$	⋯	1.2(−6)	60(−6)	⋯	1.2(−6)[b]
$A_2\ ^3\Pi_1$	0.45(−6)	52(−6)	24(−6)	1.5(−3)	0.44(−6)[c]
$A_3\ ^3\Pi_{0^-}$	⋯	0.58(−6)	⋯	⋯	0.58(−6)[c]
$A_4\ ^3\Pi_{0^+}$	6.4(−6)	1.5(−6)	⋯	76(−6)[d]	1.2(−6)

[a]Values in parentheses denote powers of ten.
[b]τ_p and τ values are estimated for SbD.
[c]τ_p and τ values are estimated at $r=3.45\ a_0\approx r_e$.
[d]τ_p value is estimated at $r=3.95\ a_0$.

the lower-lying states, namely to the $X_1 0^+$ and $X_2 1$ components of the ground state. As can be seen from Tables VI and VII, the perpendicular $b-X_2$ transition is much stronger than the parallel $b-X_1$. This result is similar to what was obtained earlier for AsH,[16] SbF,[17] or BiI,[35] but an opposite situation has been found in the calculations of BiH (Ref. 16) and SbI.[19] This distinction is closely tied up with the magnitude of the electronegativity difference of the constituent atoms in the various molecules, as has been discussed in detail in previous work.[16,19,35] A recent experimental estimate of the $b\ ^1\Sigma^+$, $v'=0$ state radiative lifetime gives 170 μs (Ref. 13) and thus is in reasonable agreement with the present calculated value of 104 μs. Some underestimation of the $\tau(b\ ^1\Sigma^+)$ value in the present study may be caused by a slightly overestimated excitation energy for the $b\ ^1\Sigma^+$ state as well as a relatively strong variation of the corresponding transition moment in the Franck–Condon region (Table VI) which makes the final τ value very sensitive to small inaccuracies in the ΔE and μ values.

The $A\ ^3\Pi$ multiplet is the only state in the low-energy SbH spectrum which has a $\Lambda-S$ allowed transition to the ground state. As a result, each Ω component of the $A\ ^3\Pi$ state has a relatively strong perpendicular transition to one of the $X\ ^3\Sigma^-$ substates, all of them characterized by similar partial lifetimes of 0.45–1.5 μs. These values are approximately equal to those for the analogous transitions in AsH, calculated to lie in the 0.6–1.3 μs range,[16] which shows that spin–orbit effects do not play any important role for such processes. The situation is quite different for the parallel $A\ ^3\Pi-X\ ^3\Sigma^-$ transitions, which become allowed due to spin–orbit coupling. As one can see from Tables VI and VII, they are noticeably weaker than those of perpendicular type, but are already much stronger than the corresponding transitions in AsH, which have τ values larger than 100 μs.[16] This is especially true for the $A_4 0^+$ state, which is strongly influenced by the spin–orbit interaction and thus has a fairly strong parallel transition to the $X_1 0^+$ state with a partial lifetime of 6.4 μs. It is also necessary to recall that we have not found any vibrational levels in the shallow $A_2 1$ and $A_3 0^-$ potential wells and therefore τ values given for these states in Table VII are only estimates obtained at their approximate equilibrium distances. It is also worth noting that the $v'=1$ vibrational level of the $A_4 0^+$ state has twice as short a partial lifetime (0.75 μs) for transition to the $X_2 1$ state as the $v'=0$ level, and the computed τ value for the $v'=2$ level is 0.83 μs. These results are consistent with the experimental finding that the strongest bands are observed for the $A\ ^3\Pi_{0^+}-X_2 1$ transition,[5] whereby the $A\ ^3\Pi_{0^+}$ state of Ref. 5 corresponds to the $A_4 0^+$, $v'=1$ level of the present study, while the $B0^+$ and $C0^+$ states are identified with the $A_4 0^+$, $v'=0$ and 2 levels, respectively (see Sec. III B 3). As can be seen from Table VII, the $A_1 2$ and $A_2 1$ states also have fairly strong transitions to the $a\ ^1\Delta$ state, which might prove useful for an experimental investigation of the metastable $a\ ^1\Delta$ state.

Similar to what has been found earlier for AsH,[16] by far the strongest transitions to the ground state are exhibited by the SbH Rydberg states, the lowest of them, the $3\ ^3\Pi$ multiplet, appearing at an excitation energy of $\sim 45 \times 10^3$ cm^{-1}. To get a better idea of their strength, one can take as a typical example the $3\ ^3\Pi_{0^+}\rightarrow X_2\ ^3\Sigma_1^-$ perpendicular transition, the partial lifetime for which has been estimated in the present study to be 11 ns. Some of the higher-lying Rydberg states of SbH (see Sec. III B 4) have already been found spectroscopically,[6] but observation of the others may encounter difficulties since many of them are predissociated near their minima due to potential crossings with the repulsive limbs of the lower-lying valence states (Figs. 4–7).

V. CONCLUSION

A CI treatment of the electronic structure and spectrum of the SbH radical has been carried out with the aid of a relativistic effective core potential for the antimony atom, including SO coupling effects. The calculated spectroscopic constants for the low-lying states of SbH are in good agreement with the available experimental data. The present computed equilibrium distances are slightly (by 0.01–0.03 Å) larger than the experimental values, and the corresponding vibrational frequencies are found to be slightly (by $\leqslant 40$ cm^{-1}, or less than 2%) underestimated. Both effects are probably due to the absence of an explicit treatment of the Sb atom $4d$ electrons in the present computational approach and have also been observed in the analogous studies of the SbO (Ref. 18) and SbI (Ref. 19) molecules, in which the same Sb RECP has been employed. They are similar for all states considered, however, and thus should not noticeably influence the relative positions of these states. The $a\ ^1\Delta$ and $b\ ^1\Sigma^+$ states are calculated to lie 370–550 cm^{-1} higher than determined experimentally, but a significant improvement is achieved in this respect in comparison with the only previous *ab initio* study of this system.[14]

Although the spin–orbit interaction in the SbH radical is noticeably stronger than in the lighter isovalent AsH system, its influence on the three lowest $\Lambda-S$ states, $X\ ^3\Sigma^-$, $a\ ^1\Delta$, and $b\ ^1\Sigma^+$, is a second-order effect and therefore is relatively weak. This interaction is naturally much stronger for the $A\ ^3\Pi$ multiplet and leads to a splitting of 2948 cm^{-1} between the $A_1 2$ and $A_4 0^+$ components. Even more important is the fact that spin–orbit interaction causes strong predissociation of the $A_1 2$, $A_2 1$, and $A_3 0^-$ substates through avoided crossings with the corresponding Ω components of the $^5\Sigma^-$ state. The $A_4 0^+$ is the most stable of the $A\ ^3\Pi$ substates, but possesses a very unusual potential energy curve with a double minimum and a fairly low barrier to dissociation. On the basis of vibrational analysis performed for this state (Sec. III), one can conclude that the experimentally observed $B0^+$ (in SbH and SbD) and $C0^+$ (in SbD) states[5] should be assigned to the $v'=0$ and 2 vibrational levels of the $A_4 0^+$ state, while the $A\ ^3\Pi_{0^+}$ state should correspond to the $v'=1$ level. This inference also agrees with the computed relative strengths of transitions to these states from the X_1 and X_2 ground state components.

The calculated radiative lifetimes of most of the SbH low-lying states are quite long, with a clear dominance of the $\Lambda-S$ allowed transitions in the low-energy electronic spectrum of this system. This situation is similar to what was found earlier for the AsH radical,[16] but different from the

BiH case,[15] where very strong spin–orbit interaction leads to comparable intensities of the spin-allowed and -forbidden transitions. For the $b-X$ transition it has been found that the parallel $b-X_1$ branch has a much longer lifetime of 16 ms than the perpendicular $b-X_2$ ($\tau_p=105\ \mu$s). This is once again analogous to the results of our calculations for AsH,[16] but opposite to the BiH $b-X_1/b-X_2$ lifetime ratio,[15] and this result can be explained by the different electronic density distribution in these systems. Potential energy curves have also been obtained for a number of higher-lying states, and we hope that they will prove useful for future experimental and theoretical studies of this radical.

ACKNOWLEDGMENTS

The authors are very grateful for numerous discussions with Professor E. H. Fink and Dr. O. Shestakov during the course of the present study. This work was supported in part by the Deutsche Forschungsgemeinschaft in the form of a Forschergruppe grant and within the Schwerpunktprogramm *Theorie relativistischer Effekte in der Chemie und Physik schwerer Elemente*. The financial support of the Fonds der Chemischen Industrie is also hereby gratefully acknowledged. O.B. is an Alexander von Humboldt-Fellow 1996–1997 and is grateful for its financial support.

[1] W. Hack, in *Gmelin Handbook of Inorganic and Organometallic Chemistry* (Springer, Berlin, 1993), N Suppl., Vol. B1, p. 14.
[2] W. Behrendt, U. W. Gerwarth, R. Haubold, J. v. Jouanne, H. Keller-Rudek, D. Koshel, H. Schäfer, and J. Wagner, in *Gmelin Handbook of Inorganic and Organometallic Chemistry* (Springer, Berlin, 1993), P Suppl., Vol. C1, p. 2.
[3] P. Bollmark and B. Lindgren, Chem. Phys. Lett. **1**, 480 (1967).
[4] N. Basco and K. K. Yee, Spectrosc. Lett. **1**, 13 (1968).
[5] P. Bollmark and B. Lindgren, Phys. Scr. **10**, 325 (1974).
[6] P. Bollmark, B. Lindgren, and U. Sassenberg, Phys. Scr. **24**, 542 (1981).
[7] V. Stackmann, K. Lipus, and W. Urban, Mol. Phys. **80**, 635 (1993).
[8] R. D. Urban, K. Essig, and H. Jones, J. Chem. Phys. **99**, 1591 (1993).
[9] M. Beutel, K. D. Setzer, O. Shestakov, and E. H. Fink, Chem. Phys. Lett. **249**, 183 (1996).
[10] M. Beutel, K. D. Setzer, O. Shestakov, and E. H. Fink, J. Mol. Spectrosc. **178**, 165 (1996).
[11] M. Beutel, K. D. Setzer, O. Shestakov, and E. H. Fink, J. Mol. Spectrosc. (to be published).
[12] M. Beutel, K. D. Setzer, O. Shestakov, and E. H. Fink, J. Mol. Spectrosc. **179**, 79 (1996).
[13] O. Shestakov and E. H. Fink (private communication).
[14] K. Balasubramanian, N. Tanpipat, and J. E. Bloor, J. Mol. Spectrosc. **124**, 458 (1987).
[15] A. B. Alekseyev, R. J. Buenker, H.-P. Liebermann, and G. Hirsch, J. Chem. Phys. **100**, 2989 (1994).
[16] A. B. Alekseyev, H.-P. Liebermann, G. Hirsch, and R. J. Buenker, J. Chem. Phys. **108**, 2028 (1998).
[17] I. Boustani, S. N. Rai, H.-P. Liebermann, A. B. Alekseyev, G. Hirsch, and R. J. Buenker, Chem. Phys. **177**, 45 (1993).
[18] A. B. Alekseyev, H.-P. Liebermann, R. J. Buenker, and G. Hirsch, J. Chem. Phys. **102**, 2539 (1995).
[19] K. K. Das, A. B. Alekseyev, H.-P. Liebermann, G. Hirsch, and R. J. Buenker, Chem. Phys. **196**, 395 (1995).
[20] L. A. LaJohn, P. A. Christiansen, R. B. Ross, T. Atashroo, and W. C. Ermler, J. Chem. Phys. **87**, 2812 (1987).
[21] G. C. Lie and E. Clementi, J. Chem. Phys. **60**, 1275 (1974).
[22] C. E. Moore, Arch. U.S. Natl. Bur. Stand. No. 467, Vol. 3 (1971).
[23] R. J. Buenker and S. D. Peyerimhoff, Theor. Chim. Acta **35**, 33 (1974); **39**, 217 (1975); R. J. Buenker, S. D. Peyerimhoff, and W. Butscher, Mol. Phys. **35**, 771 (1978).
[24] E. R. Davidson, in *The World of Quantum Chemistry*, edited by R. Daudel and B. Pullman (Reidel, Dordrecht, 1974), p. 17.
[25] G. Hirsch, P. J. Bruna, S. D. Peyerimhoff, and R. J. Buenker, Chem. Phys. Lett. **52**, 442 (1977); D. B. Knowles, J. R. Alvarez-Collado, G. Hirsch, and R. J. Buenker, J. Chem. Phys. **92**, 585 (1990).
[26] R. J. Buenker and R. A. Philips, J. Mol. Struct.: THEOCHEM **123**, 291 (1985).
[27] A. B. Alekseyev, H.-P. Liebermann, R. J. Buenker, G. Hirsch, and Y. Li, J. Chem. Phys. **100**, 8956 (1994).
[28] R. J. Buenker, A. B. Alekseyev, H.-P. Liebermann, R. Lingott, and G. Hirsch, J. Chem. Phys. **108**, 3400 (1998).
[29] J. W. Cooley, Math. Comput. **15**, 363 (1961).
[30] M. Perić, R. Runau, J. Römelt, S. D. Peyerimhoff, and R. J. Buenker, J. Mol. Spectrosc. **78**, 309 (1979).
[31] A. Banerjee and F. Grein, Chem. Phys. **35**, 119 (1978).
[32] E. M. Goldfield and K. P. Kirby, J. Chem. Phys. **87**, 3986 (1987).
[33] P. J. Bruna, G. Hirsch, S. D. Peyerimhoff, and R. J. Buenker, Mol. Phys. **42**, 875 (1981).
[34] O. Gustafsson, G. Kindvall, M. Larsson, J. Senekowitsch, and P. Sigray, Mol. Phys. **56**, 1369 (1985).
[35] A. B. Alekseyev, K. K. Das, H.-P. Liebermann, R. J. Buenker, and G. Hirsch, Chem. Phys. **198**, 333 (1995).